Photocatalytic and Gas Sensitive Multiwalled Carbon Nanotube/TiO$_2$-ZnO and ZnO-TiO$_2$ Composites Prepared by Atomic Layer Deposition

László Péter Bakos [1,*], **Nóra Justh** [1], **Ulisses Carlo Moura da Silva Bezerra da Costa** [1], **Krisztina László** [2], **János László Lábár** [3], **Tamás Igricz** [4], **Katalin Varga-Josepovits** [5], **Pawel Pasierb** [6], **Elina Färm** [7], **Mikko Ritala** [8], **Markku Leskelä** [8] and **Imre Miklós Szilágyi** [1]

[1] Department of Inorganic and Analytical Chemistry, Budapest University of Technology and Economics, Szent Gellért tér 4., H-1111 Budapest, Hungary; justh.nora@gmail.com (N.J.); ulissesccosta@gmail.com (U.C.M.d.S.B.d.C.); imre.szilagyi@mail.bme.hu (I.M.S.)

[2] Department of Physical Chemistry and Materials Science, Budapest University of Technology and Economics, P.O. Box 92, H-1521 Budapest, Hungary; klaszlo@mail.bme.hu

[3] Institute for Technical Physics and Materials Science, Research Centre of Energy, Hungarian Academy of Sciences, Konkoly–Thege út 29–33., H-1121 Budapest, Hungary; labar.janos@energia.mta.hu

[4] Department of Organic Chemistry and Technology, Budapest University of Technology and Economics, Budafoki út 8., H-1111 Budapest, Hungary; igricz.tamas@gmail.com

[5] Department of Atomic Physics, Budapest University of Technology and Economics, Budafoki út 8., H-1111 Budapest, Hungary; flip@eik.bme.hu

[6] Department of Inorganic Chemistry, AGH University of Science and Technology, Mickiewicza 30., 30-059 Kraków, Poland; ppasierb@agh.edu.pl

[7] ASM Microchemistry Oy, Pietari Kalmin katu 1F2, FI-00560 Helsinki, Finland; elina.farm@helsinki.fi

[8] Department of Chemistry, University of Helsinki, P.O. Box 55, FI-00014 Helsinki, Finland; mikko.ritala@helsinki.fi (M.R.); markku.leskela@helsinki.fi (M.L.)

* Correspondence: laszlobakos@hotmail.com

check for updates

Abstract: TiO$_2$ and ZnO single and multilayers were deposited on hydroxyl functionalized multi-walled carbon nanotubes using atomic layer deposition. The bare carbon nanotubes and the resulting heterostructures were characterized by TG/DTA, Raman, XRD, SEM-EDX, XPS, TEM-EELS-SAED and low temperature nitrogen adsorption techniques, and their photocatalytic and gas sensing activities were also studied. The carbon nanotubes (CNTs) were uniformly covered with anatase TiO$_2$ and wurtzite ZnO layers and with their combinations. In the photocatalytic degradation of methyl orange, the most beneficial structures are those where ZnO is the external layer, both in the case of single and double oxide layer covered CNTs (CNT-ZnO and CNT-TiO$_2$-ZnO). The samples with multilayer oxides (CNT-ZnO-TiO$_2$ and CNT-TiO$_2$-ZnO) have lower catalytic activity due to their larger average densities, and consequently lower surface areas, compared to single oxide layer coated CNTs (CNT-ZnO and CNT-TiO$_2$). In contrast, in gas sensing it is advantageous to have TiO$_2$ as the outer layer. Since ZnO has higher conductivity, its gas sensing signals are lower when reacting with NH$_3$ gas. The double oxide layer samples have higher resistivity, and hence a larger gas sensing response than their single oxide layer counterparts.

Keywords: carbon nanotubes; titanium dioxide; zinc oxide; atomic layer deposition; photocatalysis; gas sensing

1. Introduction

Carbon nanotubes (CNTs) have attracted great interest for application in diverse fields owing to their unique chemical and physical properties. These fields include conductive and high-strength composites, energy storage and energy conversion devices, sensors, field emission displays and radiation sources, hydrogen storage media and heterogeneous catalysis [1–11]. TiO_2 and ZnO are widely researched materials in various areas, including photocatalytic wastewater treatment and hydrogen production, solar cells and gas sensing [12–21]. CNTs have been successfully used as catalyst support materials. As photocatalyst carriers they can increase the separation and migration of photogenerated electrons and holes [22–24]. Carbon nanotubes and semiconducting metal oxides have been studied in gas sensing applications, because adsorption and desorption of gas molecules on the surface results in charge transfer, which leads to change in electric resistance. The detection sensitivity to gases depends on many factors; e.g., grain size, surface composition and morphology and the target gas [25–31].

CNT-TiO_2 and CNT-ZnO composites can be prepared by various methods; e.g., hydrothermal synthesis, sputtering, chemical vapor deposition (CVD) and atomic layer deposition (ALD) [32–34]. Among them, ALD has the advantage that it allows the coating of nanostructures in a conformal and homogenous way, with a precise control of the thickness of the deposited film at the nanoscale by successive, self-terminating, gas–surface half-reactions [35–41].

Different metal oxides were already deposited on CNTs by ALD, e.g., Al_2O_3, SnO_2, V_2O_4, HfO_2, Fe_2O_3, TiO_2 and ZnO, and in some cases they were studied in gas sensing or photocatalysis applications [42–47]. Previously, it was also studied how changing the core and shell materials influence the photocatalytic activity and gas sensing properties of TiO_2-ZnO and ZnO-TiO_2 core-shell nanofibers prepared by electrospinning and ALD [48,49]. However, to the best of our knowledge, multilayer oxide coatings have not been grown on CNTs to obtain photocatalytic and gas sensitive core-shell nanocomposites.

In our research, ALD TiO_2 and ZnO metal oxide layers were grown on multi-walled CNTs, which were functionalized with hydroxyl groups (CNT-OH) serving as ALD nucleation sites. Both single and double oxide layer coated CNT composites, i.e., CNT-TiO_2 and CNT-ZnO, and CNT-TiO_2-ZnO and CNT-ZnO-TiO_2 samples, were obtained. The name indicates the sequence of the oxide ALD processes. The carbon nanotubes and the resulting CNT-metal oxide composite materials were characterized using TG/DTA, Raman spectroscopy, XRD, XPS, SEM-EDX, TEM-EELS-SAED and low temperature N_2 adsorption. Finally, the activities of the as-prepared samples as photocatalysts and NH_3 gas sensors were studied.

2. Materials and Methods

2.1. Sample Preparation

Hydroxyl functionalized multi-walled carbon nanotubes with external diameters of 30–50 nm were used as obtained (Cheap Tubes, Cambridgeport, VT, USA).

Atomic layer deposition of TiO_2 and ZnO was performed in an ASM F-120 ALD reactor by the reaction of $TiCl_4$ and $(C_2H_5)_2Zn$ with H_2O, respectively. The reactor was operated at a pressure of about 5 mbar using nitrogen as the carrier and purge gas. For one batch, 50 mg substrate powder was placed in a folded steel mesh into the reactor. The parameters of the ALD processes are summarized in Table 1. Each time, 12 nm thick films were grown. The thicknesses were approximated by X-ray reflectometry (Bruker D8 Advance) on Si reference wafers that were coated together with CNTs.

Table 1. ALD process parameters.

Deposited Oxide	Temperature/°C	Number of Cycles	Pulse Times/s			
			Metallic Precursor	N_2 Purge	Water	N_2 Purge
TiO_2	250	250	1.5	30	3	30
ZnO	200	120	3	30	3	30

2.2. Characterization

The details of the instruments and characterization methods used can be found in the Supplementary Materials. TG/DTA curves were measured in inert (N_2) and oxidizing (air) conditions with a linear temperature program (10 °C min^{-1}). To get structure data, Raman, XRD and SAED studies were done. To see the morphologies of the samples, SEM and TEM images were taken. The elemental compositions and bonding states and were investigated with XPS, EDX and EELS. Nitrogen adsorption was utilized to measure the specific surface area. The photocatalytic activity was investigated by decomposing an aqueous solution of methyl orange under UV light irradiation (spectrum: Figure S1), and P25 Degussa TiO_2 was used for reference material. NH_3 gas sensing properties were tested at different concentrations and temperatures (setup: Figures S27–S28).

3. Results and Discussion

3.1. TG/DTA

From the thermal analysis in nitrogen (Figure 1A), it can be seen that the bare OH-functionalized carbon nanotubes lose 26.1% of the initial mass, accompanied by an endothermic process. The decomposition is not significant at the early stages; thus, the ALD process can be safely performed at 200 °C for ZnO and at 250 °C for TiO_2 without damaging the carbon nanotube substrates. In Figure 1B, the thermal analysis in air shows that the exothermic combustion of the carbon nanotubes starts around 500 °C, leaving only 3.6% residual mass at 700 °C. The residue is the catalyst used for CNT preparation, which upon further annealing in air at 900 °C gets oxidized.
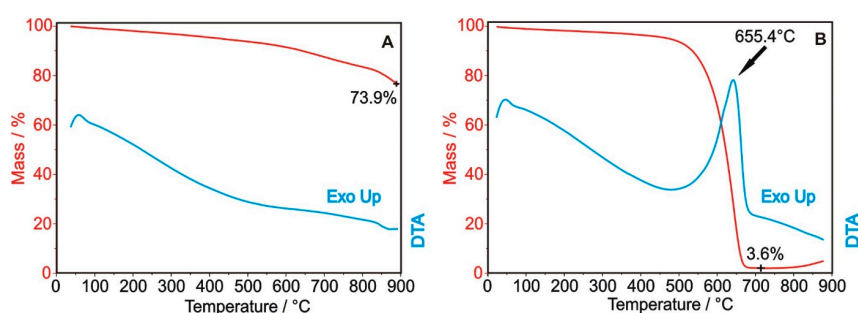

Figure 1. TG/DTA measurements of the OH-functionalized carbon nanotubes in nitrogen (**A**) and air atmospheres (**B**).

3.2. Raman Spectroscopy

The D and G peaks of the carbon are present in all samples (Figure 2). In the TiO_2 containing samples, the most intensive additional band is the TiO_2 (anatase) at 141 cm^{-1}. The further characteristic peaks of TiO_2 at 400, 516 and 637 cm^{-1} are the most obvious in the CNT-TiO_2 sample [50]. The bands of the ZnO are also detectable at 320, 428 and 569 cm^{-1}, but they are much weaker compared to the TiO_2 signals. The presence of both TiO_2 and ZnO was also verified later by XRD. In the CNT-double oxide samples both oxide signals show a reduced intensity compared with the CNTs coated by any of the single oxide layers.
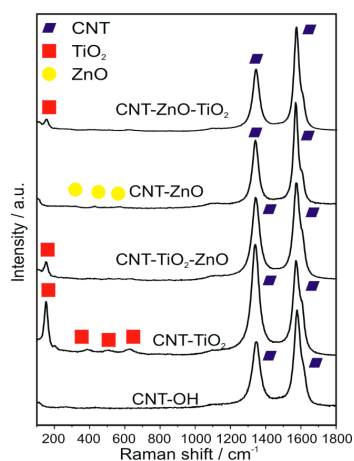
Figure 2. Raman spectra of the samples.

3.3. Powder XRD

XRD diffractograms (Figure 3) confirm the presence of the semiconductor oxides deposited on the carbon nanotubes. In the case of the bare carbon nanotubes, the peaks are characteristic of the rolled graphite layers in the multiwalled CNTs (ICDD 01-71-4630). The as-grown oxide materials are crystalline; i.e., TiO_2 is present as the anatase (ICDD 01-075-2546), and ZnO as the wurtzite (ICDD 01-080-4199), corroborating Raman spectra. Similarly to the Raman results, the oxide signals are weaker in the case of the double oxide layer coatings, than in the single oxide layer coated samples. This might imply an interaction, e.g., interdiffusion between the oxide layers, which may occur during the ALD growth of the second oxide layer. This could reduce the crystalline order of the layers, and thus, the XRD and Raman peak intensities.
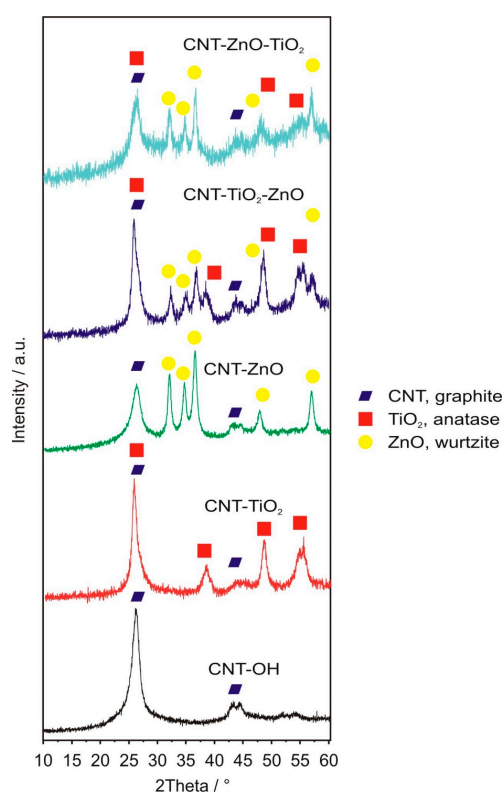

Figure 3. XRD diffractograms of the samples and the assignation of the peaks.

3.4. SEM and TEM

Figure 4 portraits SEM images of the samples after the ALD processes. The as-grown oxide layers are clearly visible on the surface of the CNTs. In the ALD reactions, both ZnO and TiO_2 nucleate as grains, and then coalesce to form a continuous layer. Since ZnO crystallizes easier than TiO_2 during the ALD depositions, it seems to form larger grains than TiO_2. In the case of the double oxide layers, the oxide coating on the CNTs becomes thicker and smoother. Based on the resolution of the SEM images, the smoothest surface was obtained in the CNT-ZnO-TiO_2 sample. The approximate diameters for the samples were around 35 nm for the CNT-OH, 50 nm for the CNT-TiO_2 and 70 nm for all the other composites.
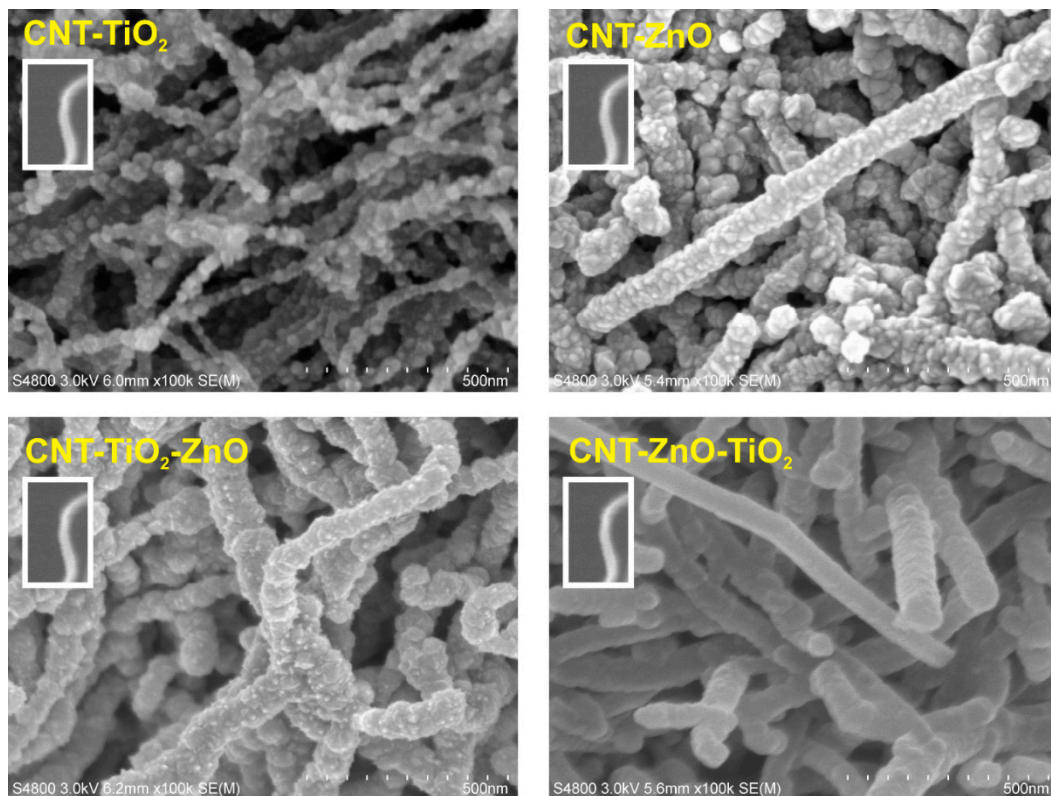

Figure 4. SEM images of the samples. In the white frame, the SEM picture of an uncoated CNT-OH is shown at the same magnification for reference.

The TEM images of the CNT-TiO_2 and the CNT-ZnO samples (Figures 5A and 5C, respectively) reveal the metal oxide layers composed of oxide nanoparticles on the carbon nanotubes. The electron diffraction patterns of the CNT-TiO_2 (Figure 5B) and CNT-ZnO (Figure 5D) samples corroborate the XRD and Raman measurements, revealing that the oxides are present as anatase and wurtzite, respectively. The TEM images of the double oxide layer coated samples (Figure 5E–I) show again that the CNTs have thicker oxide shells. The EELS maps of the C, Ti and Zn of the CNT-TiO_2-ZnO and CNT-ZnO-TiO_2 samples present the carbon core morphology surrounded by the Ti and Zn oxide layers. It is shown that the oxide layers cover the CNTs uniformly.
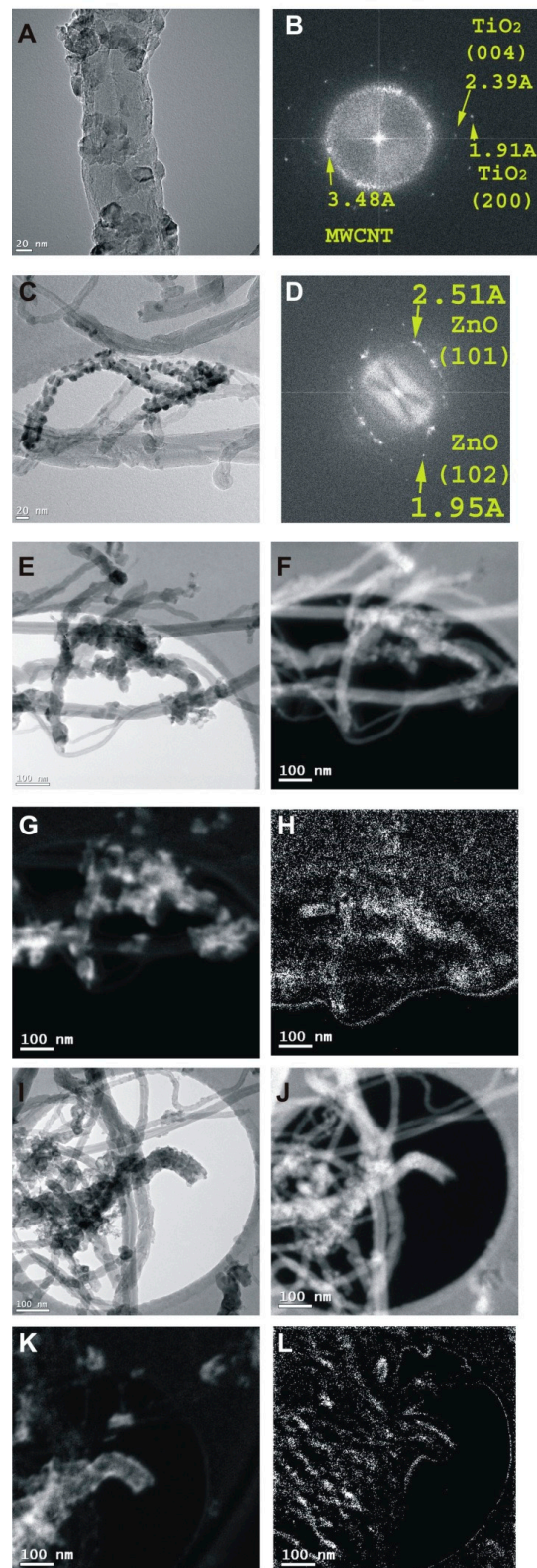
Figure 5. TEM (**A**) and FFT (**B**) of images of the CNT-TiO$_2$ sample; TEM (**C**) and FFT (**D**) of images of the CNT-ZnO sample; TEM (**E**) image and C (**F**), Ti (**G**) and Zn (**H**) EELS maps of the CNT-TiO$_2$-ZnO sample; TEM (**I**) image and C (**J**), Ti (**K**) and Zn (**L**) EELS maps of the CNT-ZnO-TiO$_2$ sample. The FFT of a TEM image has the same informational content as a SAED pattern (and is similar in appearance) from the same area.

3.5. EDX and XPS

EDX and XPS measurements also confirm that the deposition of semiconductor oxide layers was successful in the case of all samples (Table 2 and Figures S2–S27). The XPS energies of $2p_{3/2}$ peaks in all samples at 459.4 eV and at 1024.0 eV for the Ti and Zn, respectively, indicate that they are present as TiO_2 and ZnO [51,52].

Table 2. Elemental composition from EDX and XPS measurements.

Sample	EDX				XPS			
	Atomic %							
	C	O	Ti	Zn	C	O	Ti	Zn
CNT-OH	96.0	4.0			96.3	3.7		
CNT-TiO$_2$	82.0	16.2	1.8		74.7	18.8	6.5	
CNT-ZnO	92.2	7.0		0.7	82.4	8.6		9.0
CNT-TiO$_2$-ZnO	73.5	21.1	4.8	0.5	71.1	16.7	5.0	7.2
CNT-ZnO-TiO$_2$	58.2	34.3	6.6	0.9	60.0	26.2	8.4	5.4

These two methods complement each other, as XPS provides information mainly about the top 5–10 nm layer, while the information depth of EDX is ca. 0.5–1 μm. That is, XPS provides data about the very surface of the composites, and EDX, rather, about the bulk average. Accordingly, XPS measures 5–10 times higher concentration for Ti and Zn present on the surface of the CNT-oxide composite samples than EDX.

Based on the peak deconvolution (Table 3), the O1s peak of the bare CNT-OH sample contains the oxygen in two different states; i.e., the peak at 530.3 eV corresponds to the oxygen in physically adsorbed water and possible surface carbonate/carboxyl groups, while the peak at 533.0 eV is the oxygen in the OH group and chemisorbed water. The O1s peak of the coated samples at 530.8–531.2 eV comes mostly from the oxygen in the metal oxides. Compared to the bare CNT-OH, the intensity of this peak increases gradually when single and double oxide layers are grown, and simultaneously, the intensity of the OH peak between 532.2 and 532.7 decreases because the ALD reactions use up a significant amount of the OH groups [48].

Table 3. Deconvolutions of the O1s and the C1s peaks from XPS measurements.

Deconvolution of the O1s Peak									
CNT-OH		CNT-TiO$_2$		CNT-TiO$_2$-ZnO		CNT-ZnO		CNT-ZnO-TiO$_2$	
Position/eV	At. %	Position/eV	At. %	Position/eV	At. %	Position/eV	At. %	Position/eV	At. %
530.3	18.5	530.8	72.5	530.9	65.2	531.2	43.7	530.9	73.5
533.0	81.5	532.3	27.5	532.3	34.8	532.7	56.3	532.2	26.5
Deconvolution of the C1s Peak									
CNT-OH		CNT-TiO$_2$		CNT-TiO$_2$-ZnO		CNT-ZnO		CNT-ZnO-TiO$_2$	
Position/eV	At. %	Position/eV	At. %	Position/eV	At. %	Position/eV	At. %	Position/eV	At. %
284.0	72.6	284.0	61.8	284.0	66.8	284.0	63.5	284	61.1
285.3	19.7	285.1	30.8	285.3	25.1	285.2	27.6	285.2	29.5
289.4	7.7	289.5	7.4	289.6	8.1	289.8	8.9	289.5	9.4

Carbon is present in three different forms. The peak at 284.0 eV corresponds to the C–C bond, while the peak between 285.1 and 285.3 eV is related to structural defects, attributed to C atoms no longer in the regular tubular structure. The ratio of the defect related carbon increases after the ALD reactions, while the intensity of the C–C peak decreases. The signal in the 289.4–289.8 eV range is

related to the bond between C and O. Its intensity does not change significantly after the ALD processes, since most of the C–OH moieties are replaced by C–O–metal bonds [53].

3.6. Nitrogen Adsorption

The surface areas from the nitrogen adsorption measurements are shown in Table 4. The bare CNT-OH has the largest apparent surface area. After coating with a single metal oxide layer, its value decreases, and by applying a second layer, it decreases further. As the densities of the deposited oxides are significantly greater than that of the carbon nanotubes, after the ALD film growth, the average density of each sample increases. This is partly responsible for the decreasing specific surface area.

Table 4. The measurements of the specific surface areas of the samples.

Sample	CNT-OH	CNT-TiO$_2$	CNT-ZnO	CNT-TiO$_2$-ZnO	CNT-ZnO-TiO$_2$
S$_{BET}$/m^2 g^{-1}	94	54	75	43	31

3.7. Photocatalysis

All CNT-metal oxide composites possess photocatalytic activity—decomposing methyl orange (Figures 6 and 7). The CNT-ZnO sample has the best photocatalytic performance, also confirmed by the apparent reaction rate constants of the photocatalysis (Table 5) [46]. Compared to this, a significantly lower activity was observed when CNTs were coated with a TiO$_2$ layer. When the second oxide layers are grown onto the CNT-single oxide layer composites, the photocatalytic activity decreases in the case of both CNT-ZnO and CNT-TiO$_2$ substrates. The reason for this is that when the amount of heavier oxides increases compared to the lighter carbon core, the average density increases, and the surface area introduced by the 1 mg catalyst sample into the photocatalytic tests is decreased. In the case of the double layered samples, the photocatalytic results are better when ZnO is the outer layer. This is in line with the observation that the CNT-ZnO is a better photocatalyst than CNT-TiO$_2$. In fact, even the CNT-TiO$_2$-ZnO sample has higher activity than the CNT-TiO$_2$ sample.
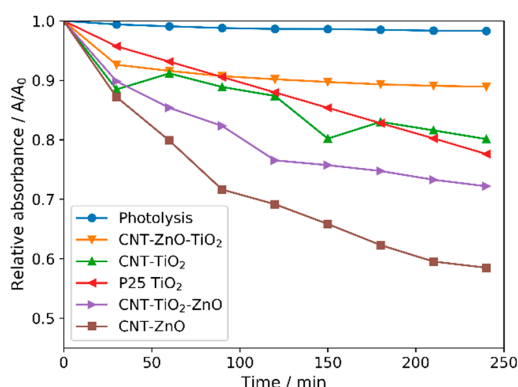

Figure 6. Photocatalytic activities of the samples.

Table 5. Results of the photocatalytic experiments.

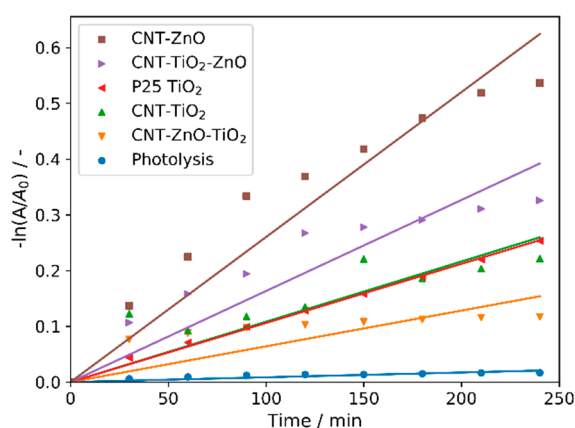| Samples	Decomposition	k$_{app}$	R^2
	%	10^{-4} min^{-1}	-
Photolysis	1.7	0.9	0.9485
P25 TiO$_2$	22.4	10.6	0.9989
CNT-TiO$_2$	19.9	10.8	0.9355
CNT-ZnO	41.5	26.0	0.9759
CNT-TiO$_2$-ZnO	27.8	16.3	0.9592
CNT-ZnO-TiO$_2$	11.1	6.4	0.8844

Figure 7. Pseudo first order linear fitting of the photocatalysis.

In case of the monolayer coated samples, the CNT core as an electron acceptor serves as a sink for the photogenerated electrons, while the holes stay in the metal oxides. This process slows the electron-hole recombination rate, thereby increasing the photocatalytic activity, as the holes can initialize the radical formation more efficiently compared to the bare metal oxides. Moreover, the metal–oxygen–carbon bonds act as sensitizers by narrowing the band gap [54,55]. Despite these effects, $CNT-TiO_2$ still performed worse than the reference P25 TiO_2, while CNT-ZnO was by far the most effective photocatalyst. For the double-layer coated composites, the obtained results correspond to former studies on $ZnO-TiO_2$ and TiO_2-ZnO core/shell nanofibers prepared by electrospinning and ALD [48,56]. The electron-hole pairs are generated mainly in the shell layers under illumination; the holes prefer the ZnO while the electrons migrate to the TiO_2. For photocatalysis the outer layer is more important, since it is in physical contact with the material to be decomposed. Therefore, photogenerated electrons are mostly responsible for the photocatalytic activity in the case of the $CNT-ZnO-TiO_2$ composite, while the photocatalysis in the presence of the $CNT-TiO_2-ZnO$ composite is controlled by the holes. To generate reactive species, the electrons have to react with oxygen, which is not abundant in the solution, while the holes react with water to produce OH radicals; thus, the ZnO outer layer is preferred. Based on previous results and our present results, higher photocatalytic activity is observed when ZnO is the outer layer than with TiO_2 being the outer one, and it is even higher than with the conventional P25 reference TiO_2. This can be explained by the surface chemistry and the intrinsic characteristics of the photogenerated charge carriers. The amount of the chemisorbed oxygen at the lattice defect sites (532.3 eV peak on XPS, Table 3) for $CNT-TiO_2-ZnO$ is 1.3 times higher than for the $CNT-ZnO-TiO_2$. ZnO may enhance the hole capture process through O defects, resulting in a lower binding energy for adsorbates, and a comparatively lower mobility of the holes in its valence band.

3.8. Gas Sensing

The gas sensing results are shown in Figure 8. An n-type NH_3 gas response is visible in all cases. The gas sensing activity is better with all samples at 25 °C than at 150 °C, because the conductivity of the semiconductors layers increases with temperature, and hence the gas responses are lower. There are small delays in the responses and recoveries for all samples at all detected gas concentrations due to the gas sensing setup volume.
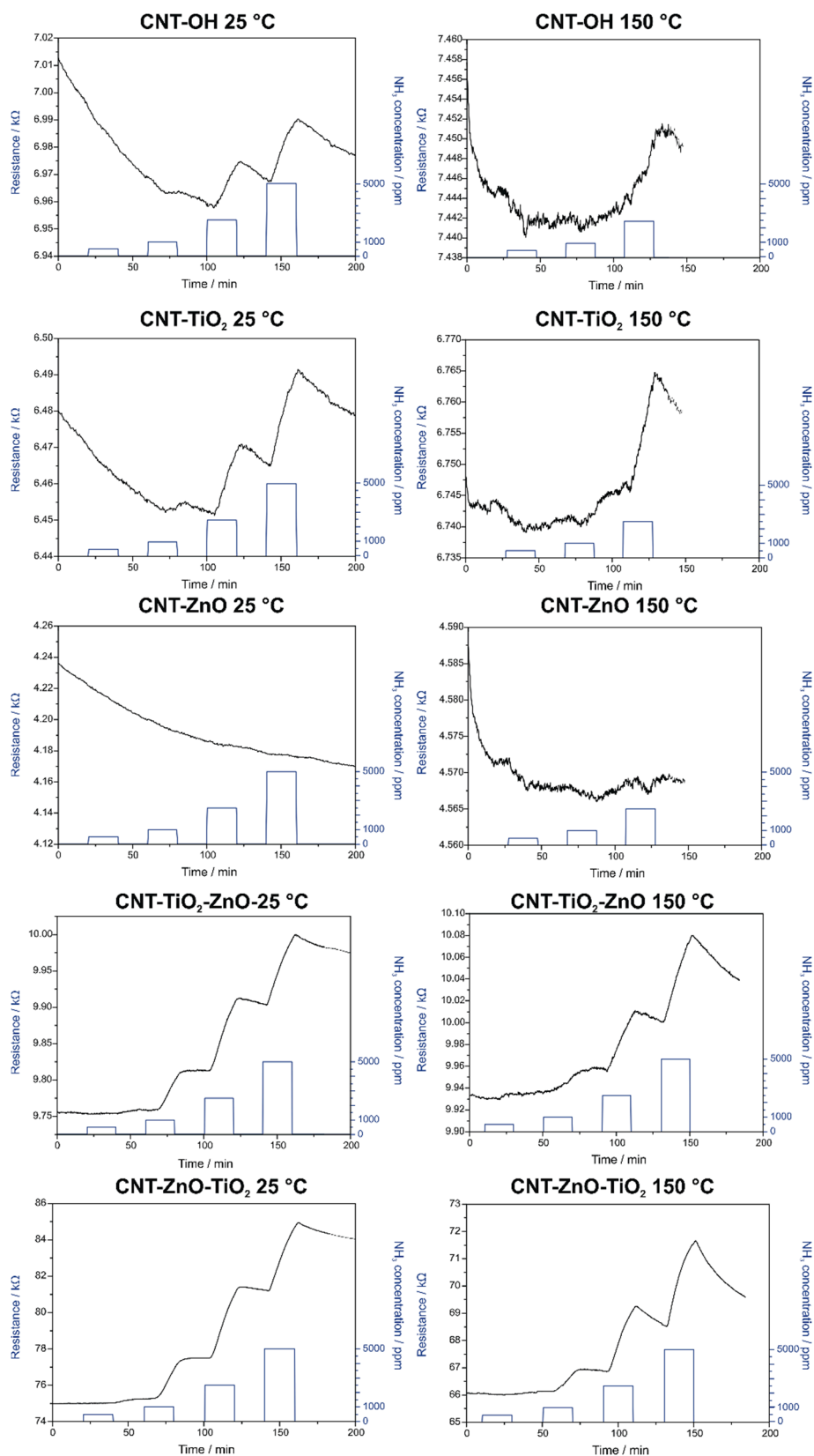
Figure 8. NH$_3$ gas sensing measurements of the various samples.

The CNT-OH sample shows a small sensitivity at room temperature, which becomes even lower at 150 °C. When ZnO is deposited on the CNTs, the surface conductivity seems to increase, which is

reflected by the decreased base resistivity, and also by the fact that that hardly any gas sensing signal is observed for this sample, even at 25 °C. When CNTs are covered with a single layer of TiO_2 by ALD, the room temperature response increases compared to that with CNT-OH, and the gas sensing property is also more pronounced at 150 °C. The resistivity of the ALD TiO_2 is often low [57,58]. Unlike the single layer oxide coatings, the CNT-multilayer oxide composites have a considerably better gas sensing performance, due to the increased resistivity of the thicker oxide shells. Because of the two layers, there is contact resistance between them, the coverage is smoother and there are less holes in the coating. In the case of these samples, it is also obvious that the order of the layers has a significant impact on the gas sensing properties. When TiO_2 is the outer layer, the response is around forty times greater at both temperatures, compared to when ZnO is the outer layer. This is explained by the lower conductivity of TiO_2 compared to ZnO. The interaction with the NH_3 gas results in a larger change in its surface resistance [59]. Therefore, in contrast to photocatalysis, for which a ZnO outer layer is more beneficial, in the case of gas sensing, it is preferable to have TiO_2 as the outer layer.

4. Conclusions

TiO_2 and ZnO single and multilayers have been successfully deposited on hydroxyl functionalized multi-walled carbon nanotubes. CNT-TiO_2, CNT-ZnO, CNT-TiO_2-ZnO and CNT-ZnO-TiO_2 core/shell nanocomposites are obtained. TG/DTA curves reveal that CNT-OH is thermally stable at the ALD temperatures; i.e., at 250 °C and 200 for TiO_2 and ZnO, respectively. EDX, XPS and Raman spectroscopy confirm the presence of the deposited oxides on the CNTs. The as-grown metal oxide layers are crystalline; i.e., TiO_2 is present as anatase and ZnO as wurtzite. SEM and TEM images show that the TiO_2 and ZnO nucleate as particles on CNTs, which merge to form uniform and continuous layers. Due to the presence of heavier oxide coating on the lighter carbon cores, the specific surface area of the nanocomposites decreases compared to the bare CNT-OH sample. The composites possess significant photocatalytic activity in decomposing methyl orange dye under UV light irradiation. The most beneficial structure is when ZnO is the outer layer, both in the case of single and double oxide layer covered CNTs. The samples with multilayer oxides have lower activity due to their larger average density and lower specific surface area. In contrast to photocatalysis, in gas sensing the advantageous structure is the one where TiO_2 is the outer layer, since ZnO has higher conductivity, and thus, its gas-sensing signals are lower than those of TiO_2 when interacting with NH_3 gas. Both the resistivity and the gas sensing signals are higher in multilayer oxide coated CNTs than either in CNT-TiO_2 or CNT-ZnO.

Author Contributions: Conceptualization, M.R., M.L. and I.M.S.; funding acquisition, M.L. and I.M.S.; investigation, N.J., U.C.M.d.S.B.d.C., K.L., J.L.L., T.I., K.V.-J., P.P. and E.F.; methodology, E.F., M.L. and I.M.S.; project administration, M.R. and M.L.; resources, M.R., M.L. and I.M.S.; supervision, I.M.S.; visualization, L.P.B.; writing—original draft, L.P.B.; writing—review and editing, N.J., U.C.M.d.S.B.d.C., K.L., J.L.L., T.I., K.V.-J., P.P., E.F., M.R., M.L. and I.M.S. All authors have read and agreed to the published version of the manuscript.

References

1. Ahmmad, B.; Kusumoto, Y.; Somekawa, S.; Ikeda, M. Carbon nanotubes synergistically enhance photocatalytic activity of TiO_2. *Catal. Commun.* **2008**, *9*, 1410–1413. [CrossRef]

2. Baughman, R.H. Carbon Nanotubes–the Route Toward Applications. *Science* **2002**, *297*, 787–792. [CrossRef] [PubMed]

3. Tóth, A.; Voitko, K.V.; Bakalinska, O.; Prykhod'ko, G.P.; Bertóti, I.; Martínez-Alonso, A.; Tascón, J.M.D.; Gun'ko, V.M.; László, K. Morphology and adsorption properties of chemically modified MWCNT probed by nitrogen, n-propane and water vapor. *Carbon N. Y.* **2012**, *50*, 577–585. [CrossRef]

4. Wang, H.; Jia, G.; Guo, Y.; Zhang, Y.; Geng, H.; Xu, J.; Mai, W.; Yan, Q.; Fan, H.J. Atomic Layer Deposition of Amorphous TiO_2 on Carbon Nanotube Networks and Their Superior Li and Na Ion Storage Properties. *Adv. Mater. Interfaces* **2016**, *3*, 1600375. [CrossRef]

5. Arash, B.; Wang, Q.; Varadan, V.K. Mechanical properties of carbon nanotube/polymer composites. *Sci. Rep.* **2015**, *4*, 6479. [CrossRef]

6. Zaporotskova, I.V.; Boroznina, N.P.; Parkhomenko, Y.N.; Kozhitov, L.V. Carbon nanotubes: Sensor properties. A review. *Mod. Electron. Mater.* **2016**, *2*, 95–105. [CrossRef]

7. Uemura, S. Carbon nanotube field emission display. In *Perspectives of Fullerene Nanotechnology*; Kluwer Academic Publishers: Dordrecht, The Netherlands, 2002; pp. 57–65.

8. Parmee, R.J.; Collins, C.M.; Milne, W.I.; Cole, M.T. X-ray generation using carbon nanotubes. *Nano Converg.* **2015**, *2*, 1. [CrossRef]

9. Cheng, H.M.; Yang, Q.H.; Liu, C. Hydrogen storage in carbon nanotubes. *Carbon N. Y.* **2001**, *39*, 1447–1454. [CrossRef]

10. Yan, Y.; Miao, J.; Yang, Z.; Xiao, F.-X.; Yang, H.B.; Liu, B.; Yang, Y. Carbon nanotube catalysts: recent advances in synthesis, characterization and applications. *Chem. Soc. Rev.* **2015**, *44*, 3295–3346. [CrossRef]

11. Voitko, K.; Tóth, A.; Demianenko, E.; Dobos, G.; Berke, B.; Bakalinska, O.; Grebenyuk, A.; Tombácz, E.; Kuts, V.; Tarasenko, Y.; et al. Catalytic performance of carbon nanotubes in H_2O_2 decomposition: Experimental and quantum chemical study. *J. Colloid Interface Sci.* **2015**, *437*, 283–290. [CrossRef]

12. Mohammadi, M.; Sabbaghi, S. Environmental Nanotechnology, Monitoring & Management Photo-catalytic degradation of 2, 4-DCP wastewater using $MWCNT/TiO_2$ nano-composite activated by UV and solar light. *Environ. Nanotechnology, Monit. Manag.* **2014**, *1–2*, 24–29.

13. Kondo, Y.; Yoshikawa, H.; Awaga, K.; Murayama, M.; Mori, T.; Sunada, K.; Bandow, S.; Iijima, S. Preparation, photocatalytic activities, and dye-sensitized solar-cell performance of submicron-scale TiO_2 hollow spheres. *Langmuir* **2008**, *24*, 547–550. [CrossRef] [PubMed]

14. Gönüllü, Y.; Rodríguez, G.C.M.; Saruhan, B.; Ürgen, M. Improvement of gas sensing performance of TiO_2 towards NO_2 by nano-tubular structuring. *Sensors Actuators B Chem.* **2012**, *169*, 151–160. [CrossRef]

15. Kumar, R.; Al-Dossary, O.; Kumar, G.; Umar, A. Zinc oxide nanostructures for NO_2 gas–sensor applications: A review. *Nano-Micro Lett.* **2015**, *7*, 97–120. [CrossRef] [PubMed]

16. Zhou, W.; Li, W.; Wang, J.Q.; Qu, Y.; Yang, Y.; Xie, Y.; Zhang, K.; Wang, L.; Fu, H.; Zhao, D. Ordered mesoporous black TiO_2 as highly efficient hydrogen evolution photocatalyst. *J. Am. Chem. Soc.* **2014**, *136*, 9280–9283. [CrossRef] [PubMed]

17. Haripriya, S.; Usmani, B.; Rogers, D.J.; Sandana, V.E.; Teherani, F.H.; Lusson, A.; Bove, P.; Drouhin, H.-J.; Razeghi, M. ZnO nanorod electrodes for hydrogen evolution and storage. *Proc. SPIE* **2012**, *8263*, 82631Y.

18. Boyadjiev, S.I.; Georgieva, V.; Yordanov, R.; Raicheva, Z.; Szilágyi, I.M. Preparation and characterization of ALD deposited ZnO thin films studied for gas sensors. *Appl. Surf. Sci.* **2016**, *387*, 1230–1235. [CrossRef]

19. Sajó, I.E.; Bakos, L.P.; Szilágyi, I.M.; Lendvay, G.; Magyari, J.; Mohai, M.; Szegedi, Á.; Farkas, A.; Jánosity, A.; Klébert, S.; et al. Unexpected Sequential NH_3/H_2O Solid/Gas Phase Ligand Exchange and Quasi-Intramolecular Self-Protonation Yield [$NH_4Cu(OH)MoO_4$], a Photocatalyst Misidentified before as $(NH_4)2Cu(MoO_4)2$. *Inorg. Chem.* **2018**, *57*, 13679–13692. [CrossRef]

20. Justh, N.; Bakos, L.P.; Hernádi, K.; Kiss, G.; Réti, B.; Erdélyi, Z.; Parditka, B.; Szilágyi, I.M. Photocatalytic hollow TiO_2 and ZnO nanospheres prepared by atomic layer deposition. *Sci. Rep.* **2017**, *7*, 4337. [CrossRef]

21. Justh, N.; Firkala, T.; László, K.; Lábár, J.; Szilágyi, I.M. Photocatalytic C60-amorphous TiO_2 composites prepared by atomic layer deposition. *Appl. Surf. Sci.* **2017**, *419*, 497–502. [CrossRef]

22. Coq, B.; Marc Planeix, J.; Brotons, V. Fullerene-based materials as new support media in heterogeneous catalysis by metals. *Appl. Catal. A Gen.* **1998**, *173*, 175–183. [CrossRef]

23. Djoki, V.R.; Marinkovi, A.D.; Ersen, O.; Uskokovi, P.S.; Petrovi, R.D.; Radmilovi, V.R.; Jana, D.T. The dependence of the photocatalytic activity of TiO_2/carbon nanotubes nanocomposites on the modification of the carbon nanotubes. *Ceram. Int.* **2014**, *40*, 4009–4018. [CrossRef]

24. Yu, Y.; Yu, J.C.; Yu, J.-G.; Kwok, Y.-C.; Che, Y.-K.; Zhao, J.-C.; Ding, L.; Ge, W.-K.; Wong, P.-K. Enhancement of photocatalytic activity of mesoporous TiO_2 by using carbon nanotubes. *Appl. Catal. A Gen.* **2005**, *289*, 186–196. [CrossRef]

25. Seiyama, T.; Kato, A.; Fujiishi, K.; Nagatani, M. A New Detector for Gaseous Components Using Semiconductive Thin Films. *Anal. Chem.* **1962**, *34*, 1502–1503. [CrossRef]

26. Wei, A.; Wang, Z.; Pan, L.-H.; Li, W.-W.; Xiong, L.; Dong, X.-C.; Huang, W. Room-Temperature NH_3 Gas Sensor Based on Hydrothermally Grown ZnO Nanorods. *Chinese Phys. Lett.* **2011**, *28*, 080702. [CrossRef]

27. Gong, J.; Li, Y.; Hu, Z.; Zhou, Z.; Deng, Y. Ultrasensitive NH_3 gas sensor from polyaniline nanograin enchased TiO_2 fibers. *J. Phys. Chem. C* **2010**, *114*, 9970–9974. [CrossRef]

28. Li, J.; Lu, Y.; Ye, Q.; Cinke, M.; Han, J.; Meyyappan, M. Carbon nanotube sensors for gas and organic vapor detection. *Nano Lett.* **2003**, *3*, 929–933. [CrossRef]

29. Szilágyi, I.M.; Saukko, S.; Mizsei, J.; Tóth, A.L.; Madarász, J.; Pokol, G. Gas sensing selectivity of hexagonal and monoclinic WO_3 to H_2S. *Solid State Sci.* **2010**, *12*, 1857–1860. [CrossRef]

30. Szilágyi, I.M.; Wang, L.; Gouma, P.I.; Balázsi, C.; Madarász, J.; Pokol, G. Preparation of hexagonal WO_3 from hexagonal ammonium tungsten bronze for sensing NH_3. *Mater. Res. Bull.* **2009**, *44*, 505–508. [CrossRef]

31. Szilágyi, I.M.; Saukko, S.; Mizsei, J.; Király, P.; Tárkányi, G.; Tóth, A.L.; Szabó, A.; Varga-Josepovits, K.; Madarász, J.; Pokol, G. Controlling the Composition of Nanosize Hexagonal WO_3 for Gas Sensing. *Mater. Sci. Forum* **2008**, *589*, 161–166. [CrossRef]

32. Bai, H.; Zan, X.; Zhang, L.; Sun, D.D. Multi-functional $CNT/ZnO/TiO_2$ nanocomposite membrane for concurrent filtration and photocatalytic degradation. *Sep. Purif. Technol.* **2015**, *156*, 922–930. [CrossRef]

33. Dong, Y.; Tang, D.; Li, C. Photocatalytic oxidation of methyl orange in water phase by immobilized TiO_2-carbon nanotube nanocomposite photocatalyst. *Appl. Surf. Sci.* **2014**, *296*, 1–7. [CrossRef]

34. Liu, J.; Li, X.; Dai, L. Water-assisted growth of aligned carbon nanotube-ZnO heterojunction arrays. *Adv. Mater.* **2006**, *18*, 1740–1744. [CrossRef]

35. Knez, M.; Nielsch, K.; Niinistö, L. Synthesis and Surface Engineering of Complex Nanostructures by Atomic Layer Deposition. *Adv. Mater.* **2007**, *19*, 3425–3438. [CrossRef]

36. Kim, H.; Lee, H.-B.-R.; Maeng, W.-J. Applications of atomic layer deposition to nanofabrication and emerging nanodevices. *Thin Solid Films* **2009**, *517*, 2563–2580. [CrossRef]

37. Parsons, G.N.; George, S.M.; Knez, M. Progress and future directions for atomic layer deposition and ALD-based chemistry. *MRS Bull.* **2011**, *36*, 865–871. [CrossRef]

38. Marichy, C.; Pinna, N. Carbon-nanostructures coated/decorated by atomic layer deposition: Growth and applications. *Coord. Chem. Rev.* **2013**, *257*, 3232–3253. [CrossRef]

39. Justh, N.; Berke, B.; László, K.; Bakos, L.P.; Szabó, A.; Hernádi, K.; Szilágyi, I.M. Preparation of graphene oxide/semiconductor oxide composites by using atomic layer deposition. *Appl. Surf. Sci.* **2018**, *453*, 245–251. [CrossRef]

40. Justh, N.; Mikula, G.J.; Bakos, L.P.; Nagy, B.; László, K.; Parditka, B.; Erdélyi, Z.; Takáts, V.; Mizsei, J.; Szilágyi, I.M. Photocatalytic properties of TiO_2@polymer and TiO_2@carbon aerogel composites prepared by atomic layer deposition. *Carbon N. Y.* **2019**, *147*, 476–482. [CrossRef]

41. Kéri, O.; Kocsis, E.; Nagy, Z.K.; Parditka, B.; Erdélyi, Z.; Szilágyi, I.M. Preparation of AL_2O_3 coated PVA and PVP nanofibers and AL_2O_3 nanotubes by electrospinning and atomic layer deposition. *Rev. Roum. Chim.* **2018**, *63*, 401–406.

42. Lee, J.S.; Min, B.; Cho, K.; Kim, S.; Park, J.; Lee, Y.T.; Kim, N.S.; Lee, M.S.; Park, S.O.; Moon, J.T. Al_2O_3 nanotubes and nanorods fabricated by coating and filling of carbon nanotubes with atomic-layer deposition. *J. Cryst. Growth* **2003**, *254*, 443–448. [CrossRef]

43. Willinger, M.-G.; Neri, G.; Bonavita, A.; Micali, G.; Rauwel, E.; Herntrich, T.; Pinna, N. The controlled deposition of metal oxides onto carbon nanotubes by atomic layer deposition: examples and a case study on the application of V_2O_4 coated nanotubes in gas sensing. *Phys. Chem. Chem. Phys.* **2009**, *11*, 3615. [CrossRef] [PubMed]

44. Meng, X.; Ionescu, M.; Banis, M.N.; Zhong, Y.; Liu, H.; Zhang, Y.; Sun, S.; Li, R.; Sun, X. Heterostructural coaxial nanotubes of CNT@Fe2O3 via atomic layer deposition: Effects of surface functionalization and nitrogen-doping. *J. Nanoparticle Res.* **2011**, *13*, 1207–1218. [CrossRef]

45. Meng, X.; Zhong, Y.; Sun, Y.; Banis, M.N.; Li, R.; Sun, X. Nitrogen-doped carbon nanotubes coated by atomic layer deposited SnO_2 with controlled morphology and phase. *Carbon N. Y.* **2011**, *49*, 1133–1144. [CrossRef]

46. Huang, S.; Liao, S.-Y.; Wang, C.-C.; Kei, C.-C.; Gan, J.-Y.; Perng, T.-P. Direct formation of anatase TiO_2 nanoparticles on carbon nanotubes by atomic layer deposition and their photocatalytic properties. *Nanotechnology* **2016**, *27*, 405702. [CrossRef]

47. Li, X.L.; Li, C.; Zhang, Y.; Chu, D.P.; Milne, W.I.; Fan, H.J. Atomic layer deposition of ZnO on multi-walled carbon nanotubes and its Use for synthesis of CNT-ZnO heterostructures. *Nanoscale Res. Lett.* **2010**, *5*, 1836–1840. [CrossRef]

48. Kayaci, F.; Vempati, S.; Ozgit-Akgun, C.; Donmez, I.; Biyikli, N.; Uyar, T. Selective isolation of the electron or hole in photocatalysis: ZnO-TiO_2 and TiO_2-ZnO core-shell structured heterojunction nanofibers via electrospinning and atomic layer deposition. *Nanoscale* **2014**, *6*, 5557–6188. [CrossRef]

49. Boyadjiev, S.I.; Kéri, O.; Bárdos, P.; Firkala, T.; Gáber, F.; Nagy, Z.K.; Baji, Z.; Takács, M.; Szilágyi, I.M. Applied Surface Science TiO_2/ZnO and ZnO/TiO_2 core/shell nanofibers prepared by electrospinning and atomic layer deposition for photocatalysis and gas sensing. *Appl. Surf. Sci.* **2017**, *424*, 190–197. [CrossRef]

50. Šćepanović, M.J.; Grujić-Brojčin, M.; Dohčević-Mitrović, Z.D.; Popović, Z. V Characterization of anatase TiO_2 nanopowder by variable-temperature Raman spectroscopy. *Sci. Sinter.* **2009**, *41*, 67–73. [CrossRef]

51. Diebold, U. TiO_2 by XPS. *Surf. Sci. Spectra* **1996**, *4*, 227. [CrossRef]

52. Islam, M.N.; Ghosh, T.B.; Chopra, K.L.; Acharya, H.N. XPS and X-ray diffraction studies of aluminum-doped zinc oxide transparent conducting films. *Thin Solid Films* **1996**, *280*, 20–25. [CrossRef]

53. Datsyuk, V.; Kalyva, M.; Papagelis, K.; Parthenios, J.; Tasis, D.; Siokou, A.; Kallitsis, I.; Galiotis, C. Chemical oxidation of multiwalled carbon nanotubes. *Carbon N. Y.* **2008**, *46*, 833–840. [CrossRef]

54. Woan, K.; Pyrgiotakis, G.; Sigmund, W. Photocatalytic Carbon-Nanotube-TiO_2 Composites. *Adv. Mater.* **2009**, *21*, 2233–2239. [CrossRef]

55. Jiang, L.; Gao, L. Fabrication and characterization of ZnO-coated multi-walled carbon nanotubes with enhanced photocatalytic activity. *Mater. Chem. Phys.* **2005**, *91*, 313–316. [CrossRef]

56. Sakthivel, S.; Neppolian, B.; Shankar, M.V.; Arabindoo, B.; Palanichamy, M.; Murugesan, V. Solar photocatalytic degradation of azo dye: comparison of photocatalytic efficiency of ZnO and TiO_2. *Sol. Energy Mater. Sol. Cells* **2003**, *77*, 65–82. [CrossRef]

57. Pore, V.; Ritala, M.; Leskelä, M.; Areva, S.; Järn, M.; Järnström, J. H_2S modified atomic layer deposition process for photocatalytic TiO_2 thin films. *J. Mater. Chem.* **2007**, *17*, 1361–1371. [CrossRef]

58. Pore, V.; Rahtu, A.; Leskelä, M.; Ritala, M.; Sajavaara, T.; Keinonen, J. Atomic Layer Deposition of Photocatalytic TiO_2 Thin Films from Titanium Tetramethoxide and Water. *Chem. Vap. Depos.* **2004**, *10*, 143–148. [CrossRef]

59. Park, J.Y.; Choi, S.W.; Lee, J.W.; Lee, C.; Kim, S.S. Synthesis and gas sensing properties of TiO_2-ZnO core-shell nanofibers. *J. Am. Ceram. Soc.* **2009**, *92*, 2551–2554. [CrossRef]